Correlated TKD/EDS - TEM - APT analysis on selected interfaces of CoSi2 thin films

H. Zschiesche, A.P.C. Campos, C. Dominici, L. Roussel, A. Charai, D. Mangelinck, C. Alfonso

Correlated TKD/EDS - TEM - APT analysis on selected interfaces of $CoSi_2$ thin films

H. Zschiesche[a,*], A. P. C. Campos[b], C. Dominici[b], L. Roussel[a], A. Charai[a], D. Mangelinck[a], C. Alfonso[a]

[a] *Aix-Marseille Université, IM2NP, CNRS, Faculté de Saint-Jérôme, Case 142, 13397 Marseille Cedex 20, France*
[b] *Aix-Marseille Université, CP2M, Faculté de Saint-Jérôme, Case 142, 13397 Marseille Cedex 20, France*

Abstract

Correlative analysis is a powerful way to relate crystallographic and chemical information to the properties of materials. In this work, a procedure is proposed to select and analyze interfaces of polycrystalline thin film materials through correlative transmission Kikuchi diffraction/energy dispersive X-ray diffraction (TKD/EDS), transmission electron microscopy (TEM) and atom probe tomography (APT). TKD provides information on the crystallographic orientation. The EDS analysis performed together with TKD in the scanning electron microscope (SEM) makes chemical information available allowing phases of similar crystal structure, but with a different composition to be distinguished. The information of TKD/EDS can be correlated to successive TEM and APT analysis on selected interfaces for structural and chemical analysis at the atomic scale. An interface of an epitaxial orientated grain of a polycrystalline $CoSi_2$ thin film on (111)Si is selected and analyzed. The selected interface has a twin character and shows facets of different orientation and area. Site-specific segregation of Ge to junctions of the facets is evidenced. The correlation between local strain from misfit (defects) at the interface and segregation is discussed.

*Corresponding author: Hannes Zschiesche
Email address: hannes.zschiesche@im2np.fr (H. Zschiesche)

Keywords: site-specific sample preparation, thin films, interfaces/interphases, transmission Kikuchi diffraction/energy-dispersive X-ray spectroscopy, transmission electron microscopy, atom probe tomography

1. Introduction

The properties of thin films can be affected by interface behavior and defects like grain boundaries. Studies of the structure and the chemistry of interfaces at the atomic scale are necessary to understand their influence on properties such as: electrical properties like work function [1], recombination in solar cells [2], magnetic properties [3], or mechanical properties [4]. Changes in structure and chemistry particularly showed the ability to alter the electrical activity of a specific grain boundary [5].

Furthermore, preferential orientations of thin films may be changed by adding elements during deposition as an interlayer or as alloying elements. For example, this was shown for $CoSi_2$ thin films on Si substrates [6] used in microelectronic applications as contact material beside $TiSi_2$ and NiSi films. Low electrical resistivity, high thermal stability and the good match of the crystal structure with Si are the main advantages of $CoSi_2$ [7]. The reaction of cobalt thin films with silicon substrates leads to sequential formation of Co_2Si, CoSi and $CoSi_2$ [8, 9]. From both fundamental and application points of view, it is important to identify the main diffusing species during the formation of silicide. Markers such as Si radiotracers or implanted gas atoms can be used to identify the diffusing species during silicide formation [10]. Pairs of atoms having very similar properties may also be used as tracers if they behave like isotopes. Such a well-known pair is constituted by silicon and germanium. For example, Ge has been used as a marker during reactive diffusion experiments of Ni-silicide formation [11] and can be used in the Co-silicide formation.

In general, silicide thin films are polycrystalline. Diffusion occurs mainly at grain boundaries and thus depends on the texture of such films [12]. The texture may be influenced by variations of chemistry and structure at interfaces [13].

In the sequential phase formation of thin films by diffusion-controlled growth, differences in grain boundary structure and chemistry can change the diffusion and thus the formation of the following phase in the sequence. By selecting and analyzing interfaces between thin film and substrate or grain boundaries, it is possible to evaluate the presence of segregated markers. A systematic study of their influence on the phase formation as well as the interface morphology can be obtained.

Transmission electron microscopy (TEM) [14] and atom probe tomography (APT) [15] are two complementary techniques which allow investigations of the structure and the chemistry of interfaces at the atomic scale [16, 17]. The correlation of them on the same sample region is a powerful way for quantitative analysis [18, 19, 20, 21, 22, 23]. Special sample holders have been developed in order to facilitate correlative investigations on the same sample [24, 25]. Recently, the TEM/APT correlation [26] has revealed a complex segregation patterning on a faceted grain boundary instead of the classical view of homogeneous decoration.

APT volumes are approximately truncated cones with an approximate maximum-diameter of about 100 nm. The geometry and size restrict the volume analyzed by APT to a tiny region of the sample. Due to the long preparation and measurement time [27], it is important to ensure the presence of the region of interest in the investigated volume. It is thus vital to be able to select specific interfaces from a lift-out in order to study their structure and chemistry. Site-specific lift-out methods for preparing the tip geometry needed for APT were developed to enhance the success rate for investigations on regions of interest and to benefit from the ability of APT for 3D atomic characterization [28, 24]. However, as soon as the grain size is too small for site-specific lift-out, but still too large to get with high probability interfaces of interest in the APT tip, the success rate decreases significantly. The combination of these lift-out methods with transmission Kikuchi diffraction (TKD) for preparing APT tips enables a high success rate for interfaces by placing them close to the tip apex analyzed in APT [29, 30, 31, 32]. TEM sample preparation holds additional requirements. A sample shape of a lamella is needed to ensure ho-

mogeneous thickness. Furthermore, particular orientation relation at interfaces are necessary for structural investigations by high resolution transmission electron microscopy (HRTEM) [33, 34]. Thus, a method respecting the constraints of both techniques is needed to be able to do correlative analysis on the same sample region. Recently, a method was published to combine the preparation procedures of TEM and APT in order to facilitate correlative structural and chemical analysis [35]. However, it is of great interest to develop a procedure that enables correlative analysis by TKD/energy dispersive X-ray spectroscopy (EDS), TEM and APT to benefit from their complementary information.

We present the application of successive (i) TEM lamella preparation, (ii) TKD/EDS analysis to select an interface of interest, (iii) TEM analysis, (iv) APT tip milling and (v) APT analysis. This is based on a new TEM-grid holder configuration which offers further facilitation and economy of time in sample preparation. This method is then applied to examine the segregation of Ge at the interface between $CoSi_2$ and (111)Si substrate.

2. Materials and Methods

Samples were prepared with a focused ion beam (FIB) `FEI Helios 600` dual-beam. Simultaneous TKD - EDS analyses were performed with a SEM `Zeiss Gemini 500` equipped with an electron backscatter diffraction (EBSD) detector, an EDS detector and `TEAM` and `OIM` software. Conventional TEM bright field (BF) images and diffraction analysis were done with a `TECNAI G20`. APT measurements were run with a `LEAP 3000XR` in voltage mode at 30 K with 20% pulse fraction, 200 kHz pulse frequency and 0.2 % detection rate. The investigated sample was a polycrystalline $CoSi_2$ thin film of about 280 nm in thickness grown by reactive diffusion of Co thin film with Si(111). 100 nm Co thin film were deposited by magnetron sputtering and annealed at 850 °C to form $CoSi_2$. Ge was introduced as a marker for diffusing species [11].

A conventional grid holder (Fig. 1a) was home-modified in order to hold Cu TEM-5-post half grids (Fig. 1b) during FIB sample preparation, TKD measurements and APT runs (Fig. 1c). This grid holder offers the possibility to handle two to three TEM grids at the same time. By this, up to 15 lamellas/tips can be loaded for TKD/EDS or APT analysis. Furthermore, a ledge (indicated by red arrow in Fig. 1a and 1c) allows aligning the bottom of the Cu TEM-5-post half-grids (black arrow in Fig. 1b) in order to facilitate the transfer of the TEM grids from a TEM double tilt sample holder. The dimensions of the conventional grid holder were reduced to fit in the APT chamber (Fig. 1c). In addition, the reduction of one grid holder side, which is indicated by a black arrow in Fig. 1c, was necessary to minimize signal coming from the grid holder material during TKD/EDS measurements.

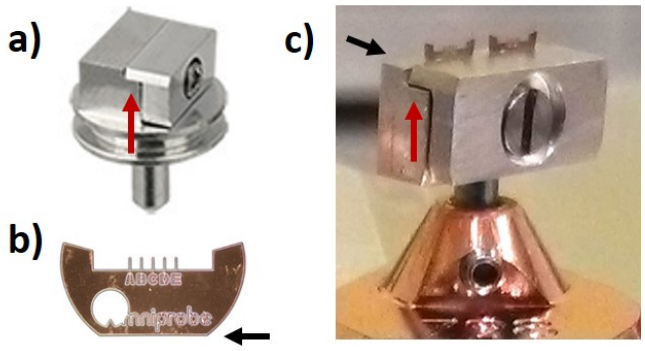

Fig. 1: Grid holder configuration. a) Conventional grid holder generally used to store TEM grids of FIB samples. A ledge (red arrow) facilitates the exchange. b) Cu TEM-5-post half grid. The bottom (black arrow) allows grid alignment at the ledge of the grid holder. c) Home-modified grid holder holding 2 grids and being placed in a conventional APT holder (bottom). One side (black arrow) was diminished minimizing signal from the grid holder in TKD/EDS analysis. The stub is thinned to fit in the conventional APT holder. This home-modified grid holder is used for FIB sample preparation, TKD/EDS and APT analysis.

The analysis procedure (TKD/EDS, TEM, APT) is applied on different sample geometries corresponding to TEM and APT. The preparation of them is a combination of TEM lamella [36] and APT tip preparation [24] using FIB. This procedure is similar to the one presented by Baik et al. [35]. Compared to

the TEM and APT classical sample preparation, two new steps are introduced: (i) Grid post preparation, lift-out and mounting on post; (ii) TEM lamella preparation and TKD analysis on the TEM lamella in order to study a selected interface by successive TEM and APT investigations.

i) Grid post preparation, lift-out and mounting on posts. Posts of the Cu TEM-5-post half grids are prepared by annular milling using a mask with an inner diameter of about 3 µm and an outer diameter of about 10 µm (Fig. 2a). High ion current is applied at 30 kV to mill a depth of 1.5 to 2 µm. The resulting local geometry is close to the one of conventional microtip arrays (coupon) [37], but surrounded by Cu from the original post shape (Fig. 2b).

A deeper milling (minimum 5 µm) of the sample during the lift-out is performed to provide a sufficient distance from the later tip apex to the post surface: this distance is needed to claim a sufficient high field effect during the APT run. Furthermore, it minimizes the probability of Cu redeposition from the TEM grid post on the sample during milling. An exact value of a minimum distance and thus depth for the lift-out can depend on the material of investigation. Comprehensive studies with a range of materials and simulations could provide a database. Care must be taken that the entered milling depth during the lift-out varies to the real milled depth depending on the calibration of the FIB and the investigated material. For example: the entered value for the lift-out in Fig. 2c was 5 µm. However, the real milling depth was measured at about 9 μm respecting a projection angle of 52° due to the stage tilt. In addition, a thick Pt layer of about 2.5 μm (measured in Fig. 2c respecting stage tilt) was deposited during lift-out process. Protecting the thin film sample from Ga contamination of the FIB ion beam by a Pt layer is especially important in final annular milling of the TEM wedge when few material remains and the region of interest can be lost easily.

The geometry of the pre-milled post facilitates the mounting of the lift-out. The moat allows a cut of the mounted lift-out without connecting the sample at the micro-manipulator with the TEM grid post due to redeposition (Fig. 2c).

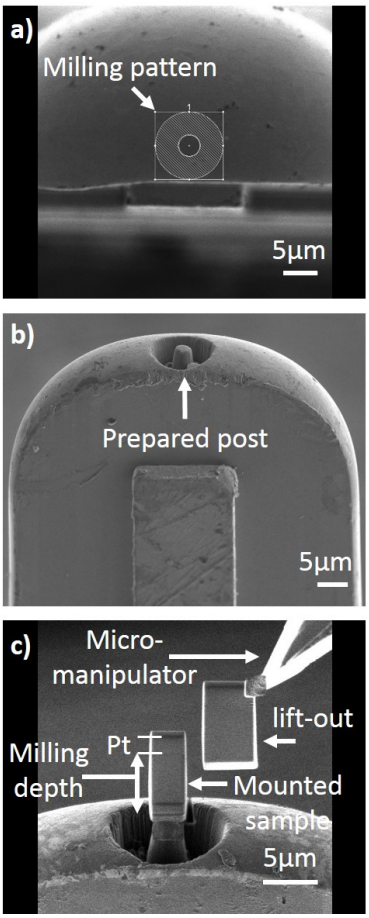

Fig. 2: Preparation of TEM-grid post and mounting of sample on it from a lift-out. a) Ion-image top view on post: Pattern milling creates a geometry applicable for APT analysis. b) Electron image side view on post: Post prepared by FIB. c) Ion image side view on sample mounted on prepared post and remaining lift-out at the micromanipulator (top right): Mounting of sample facilitated due to the moat avoiding connection of the sample at the micromanipulator with the TEM grid post by redeposition during the cut.

ii) TKD analysis on the TEM lamella. The lamella geometry offers a homogeneous thickness along the width. TKD can be performed on it and the orientation relation between two grains in the thin film or between a grain and the substrate can be determined. To select interfaces for HRTEM investigations, it is of interest to know if the sample can be orientated to get both adjacent

crystals simultaneously in low index zone axes orientation in order to resolve the atomic structure. For that, the rotation axis between adjacent crystals has to be parallel to a low index zone axis (both crystals in the same low index zone axis) or perpendicular to two low index zone axes for which the rotation angle corresponds to the angle between two low index zone axes (crystals in two different low index zone axes). In order to be able to resolve the atomic structure of the interface, the interface plane must be parallel to the viewing direction additionally. Like this, a selection of pure tilt or pure twist interfaces is obtained. The rotation axis and angle of interfaces can be determined with the software `OIM`.

After TEM and before APT analysis, the lamella must be transformed into a radial tip shape with the region of interest at the apex of the tip. Fig. 3 shows a method to do selective annular milling around a selected region. The SEM image in Fig. 3a (side view, 52° tilt) shows a TEM lamella. The substrate is at the bottom, thin film on top of it covered with protection layers of Pt. At the interface between substrate and thin film, many steps/facets can be noted (highlighted by blue arrows) since the interface is not flat. The red arrow indicates the region selected for APT tip preparation. The distances (d_l and d_r) to the borders of the lamella are measured. The distances to the borders are used during the ion milling to place the mask for radial milling around the selected region. In the presented example, the placing of the mask in relation to the selected region can be obtained between milling steps (Fig. 3b). In case that there is a flat interface without steps/facets, it is difficult to keep the milling mask over the selected region and there is a higher risk to lose the selected region during radial milling. The obtained tip containing the selected region at the apex (Fig. 3c) can be analyzed by APT.

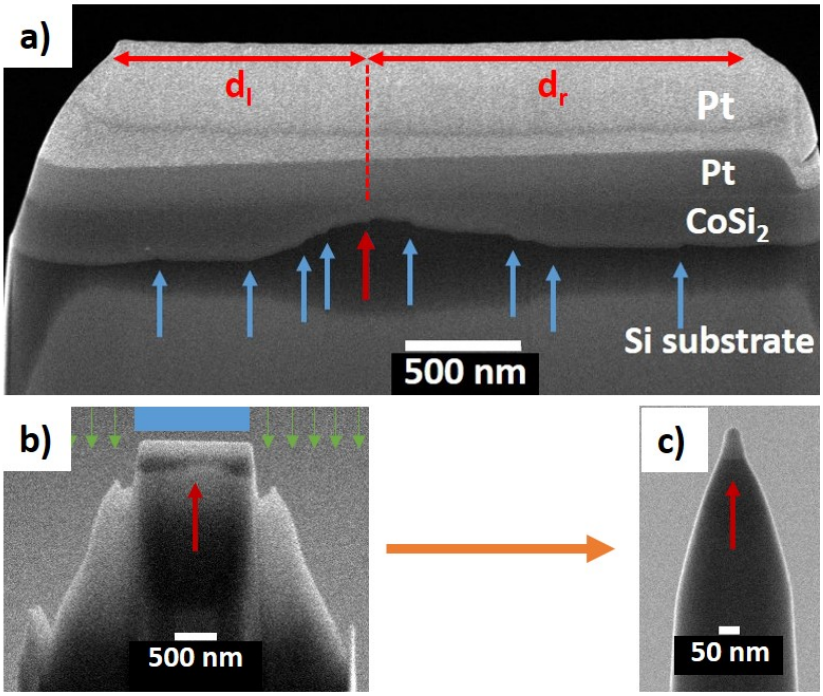

Fig. 3: Selective APT tip milling from TEM lamella. a) Selection (red arrow) of interface region from recognizing steps/facets (blue arrows). Distances (d_l and d_r) are measured to the borders of the lamella providing control of interface region selection if no steps/facets are present at the interface. b) Annular milling around selected region. Green arrows symbolize ion beam which is milling around a mask (blue bar) centered on the selected region. c) APT tip with selected region in the tip apex.

3. Results and Discussion

The results of the successive TKD/EDS, TEM and APT characterization on a $CoSi_2$ film on (111)Si with Ge markers are presented and discussed.

3.1. TKD/EDS

Fig. 4 and 5 show the EDS and TKD analysis of the TEM lamella. $CoSi_2$ (face centered cubic) and Si (diamond cubic) are both in cubic structure with similar lattice parameters (a_{Si}=5.431 Å [38], a_{CoSi_2}=5.356 Å [39]). Thus, the Kikuchi patterns are not distinguishable in TKD analysis and a correlation to

a simultaneous EDS mapping is necessary to distinguish the $CoSi_2$ thin film region and Si substrate region. The TKD analysis were thus correlated with EDS analysis simultaneously acquired in the SEM. Fig. 4a and Fig. 4b show the EDS maps of Co and Si. From regions of different compositions, the $CoSi_2$ thin film and the Si substrate can be visualized (Fig. 4c).

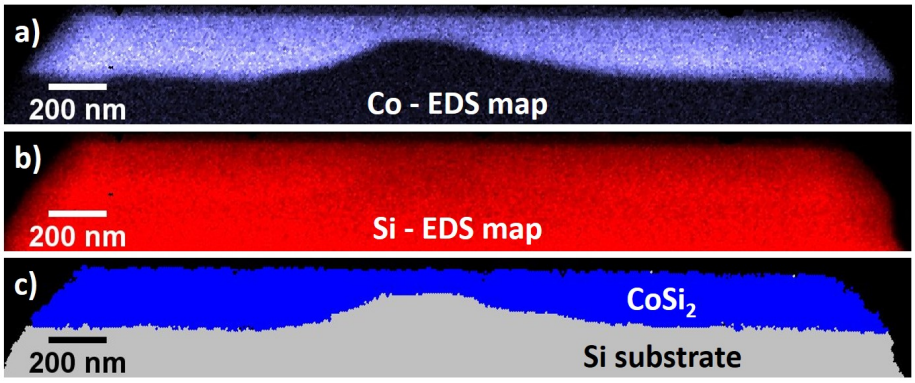

Fig. 4: EDS maps on lamella in SEM. The EDS maps of Co K a) and Si K b) localize the presence of the thin film. c) The determined compositions can be used to visualize the regions of $CoSi_2$ thin film and Si substrate.

Fig. 5 shows the TKD results in an inverse pole figure map (IPF, color code) in superposition with an image quality map (IQ, gray scale). The IQ map indicates the quality of the Kikuchi patterns by the sum of detected bands in numerical image treatments (bright region high quality, dark region low quality). Interfaces and grain boundaries appear thus darker in the IQ map. The IPF visualizes regions with orientation of identical symmetry. That means that planes of the same family are perpendicular to the viewing direction in regions of the same color. Different rotations around the viewing direction are not distinguished in the IPF. One possible distinction between the different rotations around the viewing direction is a mapping related to perpendicular viewing directions. Fig. 5a, 5b and 5c are IPFs along the perpendicular viewing directions of the reference system (RD, TD and ND). For example, the grains at the right of the imaged thin film region are all colored in a similar purple for the RD

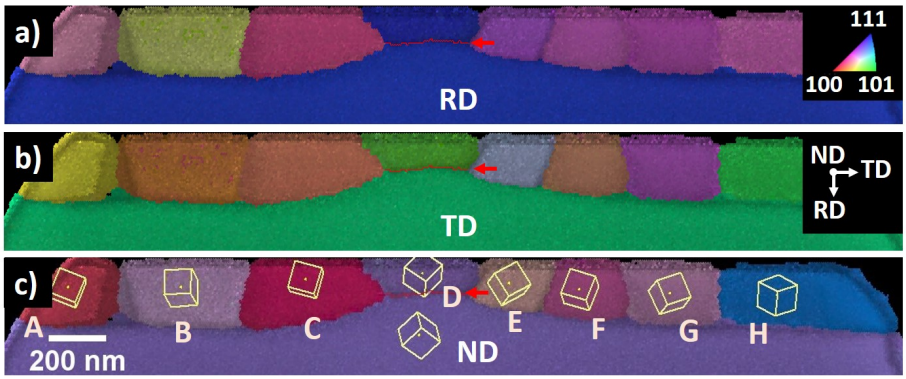

Fig. 5: TKD inverse pole figure (IPF) maps in superposition with image quality maps (IQ) on lamella in SEM. Different reference orientations are analyzed in a) (RD), b) (TD) and c) (ND). The IPF indicates orientations of the grains in a color code related to the unit triangle of the cubic structure (top right). The gray scale of the IQ indicates the quality of the Kikuchi patterns (interface and grain boundary regions appear darker).

Interface	(hkl)/[uvw] rotation axis	rotation angle Θ [°]
A	$(2\bar{2}1)/[2\bar{2}1]$	52.0
B	-	-
C	-	-
D	$(1\bar{1}0)/[1\bar{1}0]$	**70.9**
D	(111)/[111]	**180.0**
E	$(0\bar{1}1)/[0\bar{1}1]$	83.4
F	-	-
G	-	-
H	-	-

Table 1: Rotation axis and angle between substrate and grains related to Fig. 5 determined by `OIM`. Values for rotation axis and angle are listed for (hkl)/[uvw] pairs up to a norm of 4 in order to focus on low indexation. "-" is written when the norm of possible rotation axes is higher than 4.

reference direction mapping. A change of the reference direction from RD to TD and ND let appear the grains in different colors. They have no symmetric identical orientations along these reference directions. The interfaces between

the substrate and different grains are labeled from A (left) to H (right) in Fig. 5c. It can be noticed that the grain at interface D is in a similar color as the substrate for all three viewing directions. It means that grain and substrate have symmetric identical orientations in the three imaged reference directions. Thus, their structure is either identically orientated or in symmetries that cannot be distinguished from this mapping (twin, for example). Another possibility to illustrate difference of symmetric identical orientations in an IPF mapping of one reference direction is the visualization of the orientation of the unit cell from the structure. The different rotations around the same viewing direction can be determined from the detected Kikuchi patterns. For example, cubes are superimposed in Fig. 5c to the IPF. Even though the color in the IPF at the interface D is the same for both the substrate and the grain, the cubes show two different orientations with same symmetry (rotated around the viewing direction) that corresponds to a twin interface D. This twin orientation relationship of $CoSi_2$ on Si is known as epitaxy of type B_{111} [40, 41, 42] and the $CoSi_2$ grain at interface D is also named as "epitaxial $CoSi_2$ grain" in the following.

It can be noticed that the thickness of the $CoSi_2$ film is not uniform and thus present some roughness. This might be related to the microstructure of the $CoSi_2$ thin film and its growth. Indeed, the $CoSi_2$ grains with the smallest thickness (about 150 nm) correspond to the epitaxial $CoSi_2$ grain while the film thickness is larger and the substrate interface more uniform for other $CoSi_2$ grain orientations.

The rotation axis and angles of the labeled interfaces are determined and given in Tab. 1 for low index rotation axes (maximum norm 4). Only the interfaces A, D and E contain rotation axes of low indexation and are thus of interest for possible HRTEM. The rotation axis of (111)/[111] with a rotation angle of 180° (interface D) corresponds to a twin phase boundary between the epitaxial $CoSi_2$ grain and the Si substrate (red line and arrow in Fig. 5). HRTEM could be performed on the interface D in several low index zone axes (for example $(1\bar{1}0)$ and (111)). The grains of the interfaces A and E can also be in low index zone axis, but only parallel to their rotation axis. The rotation angles do

not correspond to angles between two low index zone axes perpendicular to the rotation axes.

In order to resolve the atomic structure at an interface in HRTEM, the interface plane must be parallel to the viewing direction, additionally to the fact that the atomic distances in the zone axes must be larger than the resolution limit of the used TEM. These restrictions limit the possibilities for investigations. For the following conventional TEM and APT investigations, the twin interface D was chosen.

3.2. TEM

Fig. 6 shows a TEM BF image of the TEM lamella. The microstructure of the thin film is consistent with the microstructure from the IPF-IQ (Fig. 5). The grains have a lateral size from about 200 nm to 400 nm. Thickness fringes inside the substrate parallel to the interface indicate the thickness variation of the lamella (white arrows in Fig. 6). The position of the fringes parallel to the interface and their large spacing indicate an almost constant thickness along the

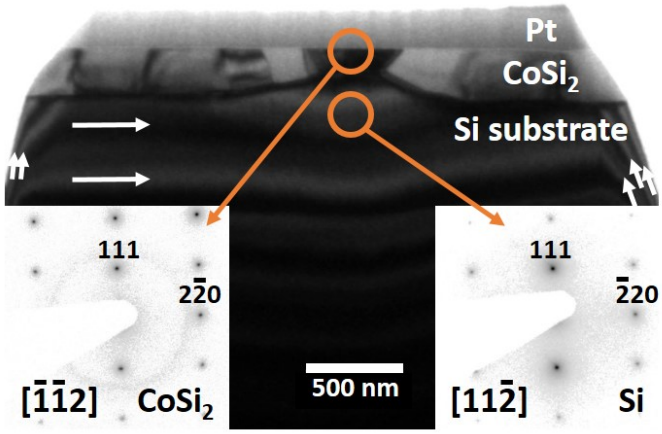

Fig. 6: TEM BF visualizing the microstructure of the thin film in cross-section. The diffraction patterns from the epitaxial $CoSi_2$ grain at interface D (bottom left) is in similar zone axis as the Si substrate (bottom right). White arrows indicate thickness fringes which are almost constant over the width of the sample.

interface direction. Furthermore, insets of diffraction patterns acquired at the epitaxial $CoSi_2$ grain (bottom left) and Si substrate (bottom right) confirm the presence of the orientation relation at the selected interface D between epitaxial $CoSi_2$ and the Si substrate. The visualized zone axis direction is parallel to $[11\bar{2}]$.

3.3. APT

A tip was prepared from the TEM lamella selecting interface D (of Fig. 5) for quantitative chemical analysis of the twin interface between epitaxial $CoSi_2$ grain and (111)Si. The reconstructed APT volume is shown in Fig. 7a. $CoSi_2$ is at the top of the volume and Si substrate at the bottom. Reconstruction parameters were optimized [43, 44] in order to get flat interface regions in agreement with TEM analysis. Interface regions can be divided in different facets. Three junctions of these facets are inside the reconstructed APT volume and marked as *J1*, *J2* and *J3* in Fig. 7a. They will be analyzed together with the chemistry at the facets after the confirmation of the orientation relation between the epitaxial $CoSi_2$ grain and the Si substrate, ensuring the analysis of the selected interface.

Since the field evaporation depends on the atomic scale local curvature, the evaporation is usually lower at special crystallographic positions such as pole positions. Crystallographic information is thus contained in the reconstructed volume and revealed by regions of different densities on the detector event hit map and consistently in the reconstructed volume. To highlight this information, 2D-density-maps of volumes perpendicular to the analysis direction have been generated in $CoSi_2$ and Si (Fig. 7b and 7c) from slides in the reconstructed volume (Fig. 7a). Both maps show the same main features. The central pole (very low density) is determined as {111} pole from the 3-fold symmetry of the zone lines (low density). In pole regions, crystal planes perpendicular to the analysis direction can be resolved (not shown). Recently, it was shown that 3D Hough transformation of a point cloud can be used to determine the orientation and periodicity of present planes [45]. This procedure has been applied on 3D APT volumes to determine the orientation of planes present in pole regions

[46]. It allows the indication of orientations of grains [47] from APT data as soon as enough crystallographic information can be obtained from the volume. The 3D Hough transformation has been applied on sub volumes (cylinders with

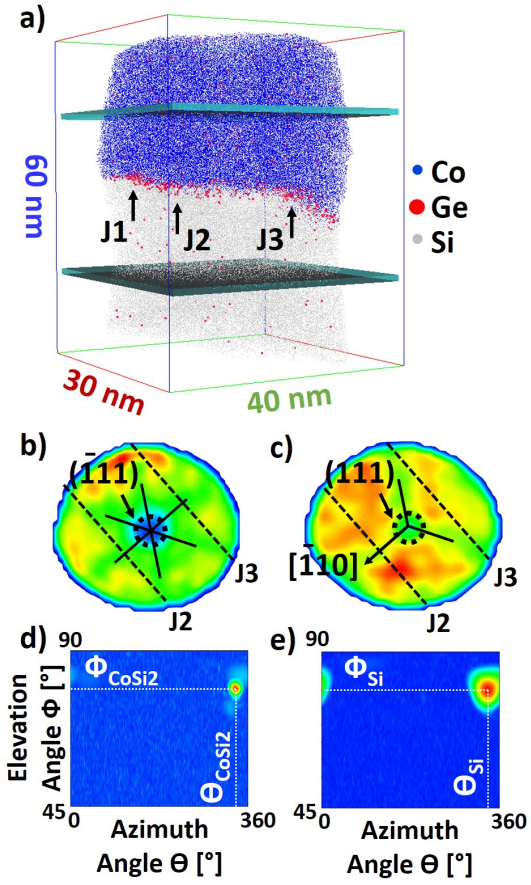

Fig. 7: APT analysis. a) The acquired volume contains an interface between $CoSi_2$ (top) and Si substrate (bottom). Junctions of the facets are marked as *J1*, *J2* and *J3*. Ge atoms are found at the interface. b) 2D density map of Co in $CoSi_2$ and c) of Si in Si. The presence of a pole is evident for thin film and substrate at about the same position in the x-y-plane which is identified as {111} pole from symmetries. The orientation of the facet junction *J1* and *J3* (dashed lines) are introduced which are perpendicular to $[1\bar{1}0]$. d), e) The periodicity maps of the 3D Hough transformation corresponding to pole regions in a) and b) verify the same orientation of the $(1\bar{1}1)$ planes in the epitaxial $CoSi_2$ grain and Si substrate.

diameter of 2 nm) in the (111) pole regions of the APT volume (indicated by circles in Fig. 7b and 7c) in order to compare the orientation of the planes of the pole in the epitaxial $CoSi_2$ grain and Si substrate. The elevation angle describes the angle between the z-axis of the reconstructed volume and the plane normal. The azimuth angle describes the angle between the x-axis of the reconstruction and the projection of the plane normal on the x-y-plane. The periodicity maps for the volumes in $CoSi_2$ (Fig. 7d) and in Si (Fig. 7e) verify that there is only one orientation of present plane normal in the elaborated pole regions. The angles corresponding to this orientation are measured to be: $\phi_{CoSi_2} = 79°$, $\theta_{CoSi_2} = 336°$ for $CoSi_2$ and $\phi_{Si} = 79°$, $\theta_{Si} = 335°$ for Si. The peak in the periodicity map for Si (Fig. 7e) is broader than the one for $CoSi_2$ (Fig. 7d). This is certainly due to the static reconstruction that was optimized to obtain a flat interface and the lattice spacing of planes in $CoSi_2$ poles instead of a dynamic reconstruction [48]. Consequently, the planes in Si appear slightly curved in the static reconstruction and this results in broader peaks in the periodicity intensity map of the 3D Hough transformation. Apart from this, the planes in the poles identified as {111} poles in the epitaxial $CoSi_2$ grain and Si have almost the same orientation in agreement with TKD/EDS and TEM analysis.

The above procedure ensures that the APT volume in Fig. 7 includes the twin interface between the epitaxial $CoSi_2$ grain and Si substrate, as chosen from the TKD investigation. A slide of the volume in Fig. 7a can be selected with its short axis in parallel to the facet junction in order to visualize the shape and chemistry of the interface by local concentration or density projection. Fig. 8 shows the localization of Ge at the interface region as a 2D Ge concentration map. In the color scale, blue means local concentration less than 0.2 at % and red higher than 1.5 at %. Assumed facets are drawn as black lines and labeled in a schematic drawing at the bottom of Fig. 8. Ge is inhomogeneously distributed at the interface. The highest amount of segregated Ge can be found at the junction *J3* (1.5 at %) followed by the junction *J1* (1.2 at %). The concentration of Ge is not significantly increased at the junction *J2* in comparison to the concentration on the adjacent facet. Ge is present in lower concentration on

the facets *F2* (about 0.6 at %) and *F4* (about 0.5 at %). Very low increase of Ge concentration (locally about 0.4 at % Ge) is detected on the facets *F1* and *F3*.

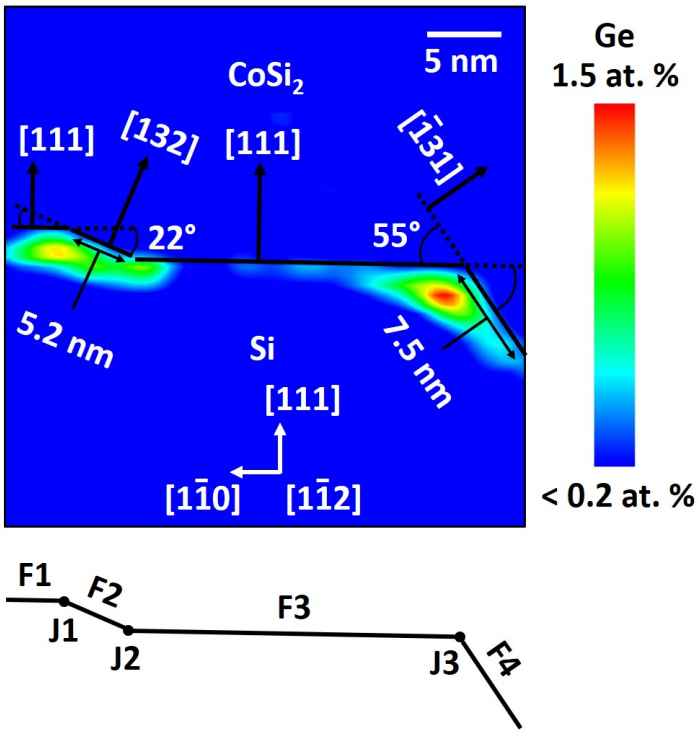

Fig. 8: 2D Ge concentration map of thin slide in Fig. 7a with viewing direction parallel to facet junctions. The Ge concentration map quantifies the distribution of Ge at the interface. Preferred places are the junctions of facets with concentration values up to 1.5 at %. Furthermore, possible indexations of facets are given on the base of measured inclination angles (assumed facet planes drawn in black lines) and the determined viewing direction. The scheme at the bottom labels facets and junctions.

As there are no indications for a grain boundary in the $CoSi_2$ (no changes in density or composition) no triple junction is present at the investigated interface region. The almost horizontal facet *F1* at the left border and the facet *F3* in the center of Fig. 8 were identified as (111) planes from comparison with the (111) pole identification. The two further facets *F2* and *F4* have different inclination angles to the (111) planes and lengths. The length of the facet *F2* is about 5.2 nm and the length of the facet *F4* is at least 7.5 nm. An indexation of these

two facets has been estimated from the crystallographic information in the APT volume as follows. It is assumed that the facet planes are perpendicular to the projection plane of Fig. 8. Thus, they have a zone axis in common which must be perpendicular to [111]. In the x-y projection from the Si-density projection along the z-axis (Fig. 7c), the $<1\bar{1}0>$ orientations can be easily determined as low-density zone lines starting from the (111) pole with a threefold symmetry (Fig. 7c) [15]. The junctions *J1* and *J3* of the facets are measured being perpendicular to one of the $<1\bar{1}0>$ orientations. Thus, the projection direction in Fig. 8 along the junctions is determined to be $[11\bar{2}]$. It represents the rotation axis which relates the (111) facets *F1* and *F3* to the other two facets *F2* and *F3* by the measured rotation angles. The inclination angle to the (111) plane is about 22° for the facet *F2* and about 55° for the facet *F4*. Candidates of lowest indexes for the facets are thus the (132) plane (22.2°) for the facet *F2* and $(\bar{1}31)$ plane (58.5°) for the facet *F4*. It must be considered that $CoSi_2$ is twin on the Si substrate. The crystal lattice is rotated by 180° around [111]. From that, the facets *F2* and *F4* correspond to the planes (312) and $(3\bar{1}1)$ in the twin $CoSi_2$, respectively.

Another quantification of the inhomogeneous Ge segregation at the interface can be given by 1D concentration profiles along cubes perpendicular to the facets. Fig. 9 shows such 1D concentration profiles: Fig. 9a, 9b, 9c correspond to profiles across the facets *F2*, *F3*, *F4* (compare insets), respectively. Cubes used for the profiles are small, and statistical fluctuation can be present. However, the interface position is clear from the change in the Si concentration profile. Clear peaks in the Ge concentration profiles with a maximum of about 1 at % are present in Fig. 9a and 9c corresponding to facets *F2* and *F4* which are different from (111). In contrast, at the (111) facet *F3* in Fig. 9b, only a small peak with a maximum of about 0.3 at % can be measured. This means the Ge concentration changes with the facet orientation. The values of the concentration values agree with the measurement from the 2D Ge concentration map in Fig. 8.

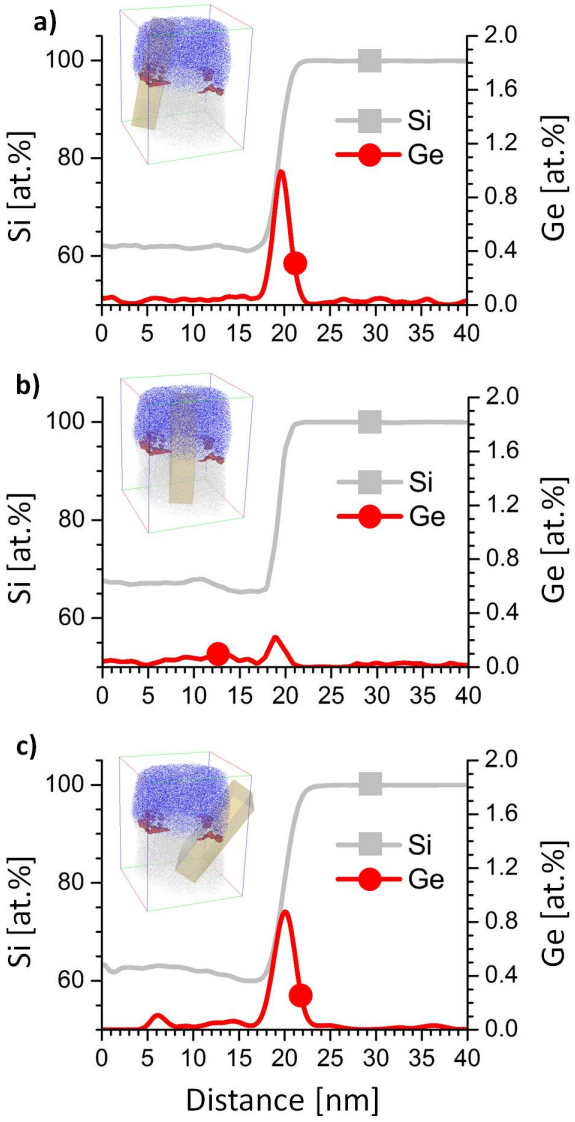

Fig. 9: Concentration profiles crossing facets of the interface indexed in Fig. 8. a) Facet [132]. b) Facet [111]. c) Facet [$\bar{1}$31]. The position of the interface in each scan is indicated by the Si concentration change. Significant Ge concentration (about 1 at %) is identified at the facets [132] and [$\bar{1}$31]. Almost no Ge segregation (about 0.3 at %) is measured at the facet [111].

4. Discussion

Stress and strain are induced at the twin interface D between the epitaxial $CoSi_2$ grain and Si due to the misfit of crystal lattice planes between $CoSi_2$ ($a_{CoSi_2} = 5.36\,\text{Å}$ [39], stretched) and Si ($a_{Si} = 5.43\,\text{Å}$ [38], compressed) [41]. Misfit dislocations [49], steps (atomic layer height) [50] or facets (accumulation of steps with a certain effective orientation) [51] can be formed in order to relax the stress. For very thin epitaxial $CoSi_2$ of type B on (111)Si, interface steps with atomic layer height were observed on the (111) interface plane by Bulle-Lieuwma et al. [41].

In our work, additional yet different facets from this (111) plane have been determined at the investigated twin interface D. All determined planes include the $[11\bar{2}]$ viewing direction of Fig. 8. Furthermore, the orientations $[11\bar{2}]$ and [111] form a mirror plane in the cubic system. This means that crystal planes of the same family are present on both sides of the twin interface D and it ensures a low misfit at all facets as crystal planes of the same family in Si and $CoSi_2$ match together (*F2*: $(312)_{CoSi_2}$ with $(132)_{Si}$; *F4*: $(3\bar{1}1)_{CoSi_2}$ with $(\bar{1}31)_{Si}$).

The orientation of the facet depends on the local energy. Interfaces can change facets due to the change of their interfacial energy by segregation of atoms [52, 53, 54]. In fact, Ge segregation has been found at the (132) facet *F2* while less Ge is present at the (111) facets *F1* and *F3*. This indicates that Ge segregation to the (132) facet lowers its interfacial energy to be equivalent to the interfacial energy of the (111) facet with a lower amount of Ge segregation. Facets different from (111) become an energetic equivalent to the (111) facet due to chemical changes.

In addition to different Ge segregation at the facets, different Ge concentration have been also determined at the junctions of the facets (Fig.8). The highest concentrations have been measured at junction *J1* and *J3* (1.2 and 1.5 at % Ge respectively) while no increase in Ge concentration compared to the adjacent facet *F2* has been found at junction *J2*.

These different segregation values could be related to different characteristics of the junctions and/or related strain fields. In particular, the opening angle in $CoSi_2$ is concave (>180°) for *J1* (202°) and *J3* (235°) but convex (<180°) for *J2* (158°). This difference should lead to varying local stress state around the junctions. From the epitaxy between $CoSi_2$ and Si and from their different structures, there should be already stress related to the epitaxy in $CoSi_2$ and in Si. This "epitaxy" stress depends on several parameters such as difference in lattice parameters, difference in thermal expansion, relaxation state... The stress field linked to the opening of the junction may either reduce or increase the stress field linked to the epitaxy. This could explain the additional segregation for concave junction while no additional segregation is found for the convex junction. Moreover, the difference between the two concave junctions seems to confirm this behavior since the additional segregation is higher for the concave junction with the highest angle (*J3*, 235°, 1.5 at % Ge) than for the lower angle junction (*J2*, 202°, 1.2 at % Ge).

This simple explanation of segregation related to the strain field around the junctions does not consider additional defects at the junction such as dislocations. For example, solute segregation to strain fields of dislocations was predicted [55], and experimental evidence was given [56, 57] and confirmed by simulations [58, 59]. For a more detailed relation of the Ge segregation to the structure at the interface, structural investigations with atomic resolution would be necessary.

Our results show that Ge segregates to specific sites (facets and in particular junctions of facets) of the interface between $CoSi_2$ and Si. It was discovered within interfaces between silicide and Si, Ge segregates site-specific to triple junction regions ([60] and therein). Triple junctions and junctions of interface facets seem thus to behave remarkably with respect to segregation. However, our work goes beyond the cited works about Ge segregation at interfaces between silicides and Si and shows site-specific segregation behavior to specific junctions and facets.

In equivalence to interfaces, grain boundaries can form facets to minimize their energy [61]. It was recently shown that impurities segregate to junctions of grain boundary facets instead of homogeneous segregation to the grain boundary facets [26]. Our work presents the counterpart for interphase. We show inhomogeneous interphase segregation to facets and junctions of facet which may be related to strain field characteristics and which could reduce interfacial energy.

In the above discussion, it was assumed that the Ge segregation corresponds to equilibrium segregation. However, diffusion may play an important role in the redistribution of Ge [60]. As the annealing temperature used to form $CoSi_2$ is relatively high, the Ge diffusion may be fast enough to reach a (quasi)equilibrium state, thus justifying our assumption.

In Fig. 4, 5 and 6, it was noticed that the epitaxial grain is thinner than the grains with other orientations. Furthermore, this behavior was found for other place in the sample: the $CoSi_2$ thin film thickness is lower in regions of epitaxial grains and larger for the other orientations. However, the initial substrate surface present negligible roughness. Thus, the difference in $CoSi_2$ thickness and the roughness of the silicide/substrate interface should have developed during the silicide formation. This might be due to different diffusion or interface motion depending on the grain orientation during the phase formation.

In particular, the epitaxial interface may have a lower mobility than an incoherent interface. Concerning intra granular (lattice) diffusion, $CoSi_2$ has a cubic structure: the lattice self-diffusion should be isotropic and thus not depend on grain orientation. However, differences in the diffusivity can result from other diffusion paths such as grain boundaries (or triple junctions). Indeed, diffusion in grain boundaries (or triple junctions) can strongly depend on their properties (misorientation, grain boundary plane, etc.). It is possible that specific grain boundaries (low misorientation for example) with lower diffusion constants are formed around the epitaxial $CoSi_2$ grain. Lower diffusion constants can lead to slower phase growth towards the substrate and thus to the development of interface roughness. That can be either due to slower Co diffusion towards

the $CoSi_2$/Si interface if Co is the main diffusion species or due to slower Si diffusion from the $CoSi_2$/Si interface to the CoSi/$CoSi_2$ interface. Furthermore, considering diffusion along the interfaces, it is possible that the diffusivities of Co and Si along interfaces with epitaxial relationship are lower than for general interfaces. It can slow down the interface growth velocity (reaction rate, interface motion) of the $CoSi_2$ phase towards the substrate and introduce the interface roughness. An additional impact can be given from Ge segregating which may change the diffusion behavior of Co and Si in grain boundaries and interfaces.

The evolution of the interface roughness during the $CoSi_2$ formation is schematically visualized in Fig. 10. A uniform polycrystalline $CoSi_2$ layer has been formed at the CoSi/Si interface (Fig. 10a). The colors of the $CoSi_2$ grains represent different orientations of which the blue one is an epitaxial $CoSi_2$ grain. The arrows indicate the growth rate. The lower growth rate at the interface between the epitaxial $CoSi_2$ grain and the Si substrate results in a strong interface roughness in which the epitaxial $CoSi_2$ grain is located on a bump.

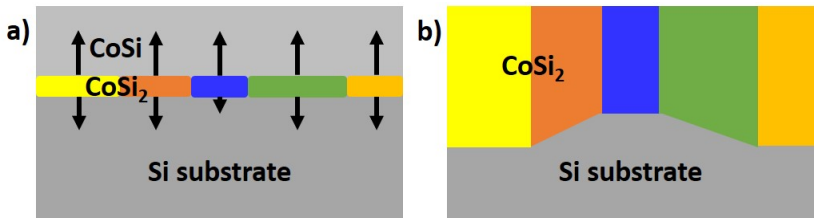

Fig. 10: Scheme of interface roughness resulting from differences in Co and/or Si diffusivity during $CoSi_2$ formation.

5. Conclusion

A procedure is proposed to perform correlative TKD/EDS-TEM-APT analysis on selected interfaces. A successful application of the procedure is presented on a twin interface between an epitaxial $CoSi_2$ grain of a polycrystalline $CoSi_2$ film and (111)Si substrate. It is demonstrated that the successive preparation of TEM lamella and APT tips offers the possibility to choose an interface

from a TKD/EDS mapping in order to analyze the structure and chemistry. The procedure can also be applied for the selection of grain boundaries as well as for systems other than thin films with an appropriate microstructure. It also offers the possibility for systematic investigation of structure and chemistry at interfaces.

When Ge is introduced as a marker, it segregates to the interface between $CoSi_2$ and Si. The investigated twin interface is composed of facets. Facet planes are observed which are different from the energetic favorable (111) plane of pure (111) twin interfaces [50]. In addition, Ge segregation to these facets is evidenced to be higher than Ge segregation to the (111) facets. It is concluded that Ge segregation locally lowers the interfacial energy. Furthermore, higher Ge segregation to junctions of facets is determined to depend on the strain field of the junctions. Thus, segregation at interfaces is site-specific and related to minimize interfacial energies.

Acknowledgment

This work was supported by the French government through the program "Investissements d'Avenir A*MIDEX" (Project APODISE, no. ANR-11-IDEX-0001-02) managed by the National Agency for Research (ANR). The authors would like to thank M. Bertoglio for assistance with sample growth, M. Descoins for assistance with APT, R. Rigard-Cerison from the laboratory PIIM Aix Marseille university for the modification of the conventional SEM TEM-grid holder, M. Cabie, L. Patout and T. Neisius for assistance with TEM and fruitful discussions, and L.C. Peters for copy editing.

References

[1] K. L. Hoyer, A. H. Hubmann, and A. Klein. Influence of dopant segregation on the work function and electrical properties of Ge-doped in comparison to Sn-doped In2O3 thin films. *Physica Status Solidi (A) Applications and Materials Science*, 214(2):1–8, 2017.

[2] C. P. Muzzillo. Review of grain interior, grain boundary, and interface effects of K in CIGS solar cells: Mechanisms for performance enhancement. *Solar Energy Materials and Solar Cells*, 172:18–24, 2017.

[3] B. B. Straumal, S. G. Protasova, A. A. Mazilkin, et al. Ferromagnetic behaviour of ZnO: The role of grain boundaries. *Beilstein Journal of Nanotechnology*, 7(1):1936–1947, 2016.

[4] S. Kobayashi, S. Tsurekawa, and T. Watanabe. A new approach to grain boundary engineering for nanocrystalline materials. *Beilstein Journal of Nanotechnology*, 7(1):1829–1849, 2016.

[5] O. Palais, A. Lamzatouar, O. B. Hardouin Duparc, et al. Correlation between electrical activity and various structures of Ge grain boundaries. *Journal of Physics Condensed Matter*, 16(2), 2004.

[6] C. Detavernier, C. Lavoie, and R. L. Van Meirhaeghe. CoSi2 formation in the presence of Ti, Ta or W. *Thin Solid Films*, 468(1-2):174–182, 2004.

[7] S. P. Murarka. Silicide thin films and their applications in microelectronics. *Intermetallics*, 3(3):173–186, 1995.

[8] S. S. Lau, J. W. Mayer, and K. N. Tu. Interactions in the Co/Si thin film system. I. Kinetics. *Journal of Applied Physics*, 49(7):4005–4010, 1978.

[9] F. M. D'Heurle and C. S. Petersson. Formation of thin films of CoSi2: Nucleation and diffusion mechanisms. *Thin Solid Films*, 128(3-4):283–297, 1985.

[10] F. M. D'Heurle and P. Gas. Kinetics of formation of silicides: A review. *Journal of Materials Research*, 1(1):205–221, 1986.

[11] M. El Kousseifi, K. Hoummada, and D. Mangelinck. Ni silicide study at the atomic scale: Diffusing species, relaxation and grooving mechanisms. *Acta Materialia*, 83:488–498, 2015.

[12] H. Mehrer. *Diffusion in solids: fundamentals, methods, materials, diffusion-controlled processes*. Springer, 2007.

[13] C. Detavernier, R. L. Van Meirhaeghe, W. Vandervorst, et al. Influence of processing conditions on CoSi2 formation in the presence of a Ti capping layer. *Microelectronic Engineering*, 71:252–261, 2004.

[14] D. B. William and C. B. Carter. *Transmission Electron Microscopy*. Springer, 2009.

[15] B. Gault, M. P. Moody, J. M. Cairney, et al. *Atom Probe Microscopy*. Springer, 2012.

[16] B. Bonef, G. Lionel, J.-L. Rouviere, et al. Atomic arrangement at ZnTe / CdSe interfaces determined by high resolution scanning transmission electron microscopy and atom probe tomography. *Applied Physics Letters*, 106(5):55–58, 2015.

[17] B. Bonef, B. Haas, J. L. Rouvière, et al. Interfacial chemistry in a ZnTe/CdSe superlattice studied by atom probe tomography and transmission electron microscopy strain measurements. *Journal of Microscopy*, 262(2):178–182, 2016.

[18] D. N. Seidman, B. W. Krakauer, and D. Udler. Atomic scale studies of solute-atom segregation at grain boundaries: Experiments and simulations. *Journal of Physics and Chemistry of Solids*, 55(10):1035–1057, 1994.

[19] O. Cojocaru-Mirédin, P. P. Choi, D. Abou-Ras, et al. Characterization of grain boundaries in Cu(In,Ga)Se2 films using atom-probe tomography. *IEEE Journal of Photovoltaics*, 1(2):207–212, 2011.

[20] T. Homma, M. P. Moody, D. W. Saxey, et al. Effect of Sn addition in preprecipitation stage in Al-Cu alloys: A correlative transmission electron microscopy and atom probe tomography study. *Metallurgical and Materials Transactions A: Physical Metallurgy and Materials Science*, 43A:2192–2202, 2012.

[21] M. Herbig, D. Raabe, Y. J. Li, et al. Atomic-scale quantification of grain boundary segregation in nanocrystalline material. *Physical Review Letters*, 112(12):1–5, 2013.

[22] A. Stoffers, J. Barthel, C. H. Liebscher, et al. Correlating Atom Probe Tomography with Atomic-Resolved Scanning Transmission Electron Microscopy: Example of Segregation at Silicon Grain Boundaries. *Microscopy and Microanalysis*, 23(2):291–299, 2017.

[23] A. Kwiatkowski da Silva, G. Leyson, M. Kuzmina, et al. Confined chemical and structural states at dislocations in Fe-9wt%Mn steels: A correlative TEM-atom probe study combined with multiscale modelling. *Acta Materialia*, 124:305–315, 2017.

[24] P. J. Felfer, T. Alam, S. P. Ringer, et al. A reproducible method for damage-free site-specific preparation of atom probe tips from interfaces. *Microscopy Research and Technique*, 75(4):484–491, 2012.

[25] M. Herbig, P. Choi, and D. Raabe. Combining structural and chemical information at the nanometer scale by correlative transmission electron microscopy and atom probe tomography. *Ultramicroscopy*, 153:32–39, 2015.

[26] C. H. Liebscher, A. Stoffers, M. Alam, et al. Strain-Induced Asymmetric Line Segregation at Faceted Si Grain Boundaries. *Physical Review Letters*, 121(1):1–5, 2018.

[27] M. K. Miller and R. G. Forbes. Atom probe tomography. *Materials Characterization*, 60(6):461–469, 2009.

[28] K. Thompson, D. Lawrence, D. J. Larson, et al. In situ site-specific specimen preparation for atom probe tomography. *Ultramicroscopy*, 107(2-3):131–139, 2007.

[29] A. J. Breen, K. Babinsky, A. C. Day, et al. Correlating Atom Probe Crystallographic Measurements with Transmission Kikuchi Diffraction Data. *Microscopy and Microanalysis*, 23(2):279–290, 2017.

[30] K. Babinsky, J. Weidow, W. Knabl, et al. Atom probe study of grain boundary segregation in technically pure molybdenum. *Materials Characterization*, 87:95–103, 2014.

[31] K. Babinsky, W. Knabl, A. Lorich, et al. Grain boundary study of technically pure molybdenum by combining APT and TKD. *Ultramicroscopy*, 159:445–451, 2015.

[32] K. P. Rice, Y. Chen, T. J. Prosa, et al. Implementing Transmission Electron Backscatter Diffraction for Atom Probe Tomography. *Microscopy and Microanalysis*, 22(3):583–588, 2016.

[33] E. F. Rauch, J. Portillo, S. Nicolopoulos, et al. Automated nanocrystal orientation and phase mapping in the transmission electron microscope on the basis of precession electron diffraction. *Zeitschrift fur Kristallographie*, 225(2-3):103–109, 2010.

[34] A. K. Kiss, E. F. Rauch, B. Pécz, et al. A Tool for Local Thickness Determination and Grain Boundary Characterization by CTEM and HRTEM Techniques. *Microscopy and Microanalysis*, 21(2):422–435, 2014.

[35] S. I. Baik, D. Isheim, and D. N. Seidman. Systematic approaches for targeting an atom-probe tomography sample fabricated in a thin TEM specimen: Correlative structural, chemical and 3-D reconstruction analyses. *Ultramicroscopy*, 184:284–292, 2018.

[36] R. M. Langford and C. Clinton. In situ lift-out using a FIB-SEM system. *Micron*, 35(7):607–611, 2004.

[37] D. J. Larson, T. J. Prosa, R. M. Ulfig, et al. *Local Electrode Atom Probe Tomography*. Springer, 2013.

[38] R. W. G. Wyckoff. Sample at T = 300 K. *Crystal Structures*, 1:7–83, 1963.

[39] R. W. G. Wyckoff. Fluorite structure. *Crystal Structures*, 1:298–444, 1963.

[40] C. W. T. Bulle-Lieuwma. Epitaxial growth of CoSi2/Si structures. *Applied Surface Science*, 68:1–18, 1993.

[41] C. W. Bulle-Lieuwma, D. E. Vandenhoudt, J. Henz, et al. Investigation of the defect structure of thin single-crystalline CoSi2(B) films on Si(111) by transmission electron microscopy. *Journal of Applied Physics*, 73(7):3220–3236, 1993.

[42] K. De Keyser, C. Detavernier, J. Jordan-Sweet, et al. Texture of CoSi2 films on Si(111), (110) and (001) substrates. *Thin Solid Films*, 519(4):1277–1284, 2010.

[43] P. Bas, A. Bostel, B. Deconihout, et al. A general protocol for the reconstruction of 3D atom probe data. *Applied Surface Science*, 87-88(1-4):298–304, 1995.

[44] F. Vurpillot, B. Gault, B. P. Geiser, et al. Reconstructing atom probe data: A review. *Ultramicroscopy*, 132:19–30, 2013.

[45] F. Tarsha-Kurdi, T. Landes, and P. Grussenmeyer. Hough-Transform and Extended Ransac Algorithms for Automatic Detection of 3D Building Roof Planes From Lidar Data. *ISPRS Workshop on Laser Scanning 2007 and SilviLaser 2007*, pages 407–412, 2007.

[46] L. Yao, M. P. Moody, J. M. Cairney, et al. Crystallographic structural analysis in atom probe microscopy via 3D Hough transformation. *Ultramicroscopy*, 111(6):458–463, 2011.

[47] V. J. Araullo-Peters, B. Gault, S. L. Shrestha, et al. Atom probe crystallography: Atomic-scale 3-D orientation mapping. *Scripta Materialia*, 66(11):907–910, 2012.

[48] B. Gault, S. T. Loi, V. J. Araullo-Peters, et al. Dynamic reconstruction for atom probe tomography. *Ultramicroscopy*, 111(11):1619–1624, 2011.

[49] J. H. Van der Merwe. Misfit dislocations in epitaxy. *Metallurgical and Materials Transactions A: Physical Metallurgy and Materials Science*, 33(8):2475–2483, 2002.

[50] C. D. Meneau and P. Perret. Cobalt disilicide growth and interface structure analyses. *Philosophical Magazine A*, 63(6):1221–1239, 1991.

[51] M. D. Rouhani, M. Sahlaoui, A. M. Gué, et al. Roughening and facetting in lattice-mismatched heteroepitaxial growth of compound semiconductors: a Monte Carlo study. *Materials Science and Engineering B-Solid State Materials for Advanced Technology*, 28(1-3):200–203, 1994.

[52] T. G. Ference and R. W. Balluffi. Observation of a reversible grain boundary faceting transition induced by changes of composition. *Scripta Metallurgica*, 22(12):1929–1934, 1988.

[53] C. W. Park and D. Y. Yoon. Singular grain boundaries in alumina and their roughening transition. *Journal of the American Ceramic Society*, 86(4):603–611, 2003.

[54] Q. Chen and N. V. Richardson. Surface facetting induced by adsorbates. *Progress in Surface Science*, 73(4-8):59–77, 2003.

[55] J. Friedel. Electronic structure of primary solid solutions in metals. *Advances in Physics*, 3(446):539–595, 1954.

[56] K. Sickafus and S. L. Sass. Observation of the effect of solute segregation on grain boundary structure. *Scripta Metallurgica*, 18(2):165–168, 1984.

[57] J. A. Eastman and S. L. Sass. Influence of Iron Solute on the Structure of Small-Angle [OOl] Twist Boundaries in Magnesium Oxide. *J. Am. Ceram. Soc.*, 69(10):753–766, 1986.

[58] D. Udler and D. N. Seidman. Solute-atom interactions with low-angle twist boundaries. *Scripta Metallurgica et Materiala*, 26:449–454, 1992.

[59] D. Udler and D. N. Seidman. Solute-atom interactions with low-angle tilt boundaries. *Scripta Metallurgica*, 26:803–808, 1992.

[60] E. Bourjot, M. Grégoire, F. Nemouchi, et al. Thermal stability of Ni(1-u) Pt(u) ($0 < u < 0.15$) germanosilicide. *Journal of Applied Physics*, 121(13), 2017.

[61] A. Stoffers, B. Ziebarth, J. Barthel, et al. Complex Nanotwin Substructure of an Asymmetric Σ9 Tilt Grain Boundary in a Silicon Polycrystal. *Physical Review Letters*, 115(23):1–5, 2015.